3 Dimensional Ferroshimming of a 25 T Resistive Magnet

Bird, M.D., NHMFL
Cross, T.A., NHMFL
Gan, Z., NHMFL
Soghomonian, V., NHMFL
Starewicz, P., Resonance Research Inc.

A 25 T resistive magnet with a field uniformity goal of 1 ppm over a 10 mm diameter spherical volume has been built at the NHMFL.[1,2] It consists of three concentric Florida-Bitter coils. The middle coil has a split of 31.8 mm at the midplane to compensate the z^2-1/2R^2 term. This simple second order correction does not provide the required uniformity of 1 ppm, due to imperfections inherent in construction of a real magnet.

For NMR applications, the relevant uniformity measurement is the variation of the magnitude of the magnetic field vector over the sample space, i.e.

$$|\vec{B}| = \sqrt{B_z^2 + B_y^2 + B_x^2} = B_z\left(1 + \frac{B_y^2 + B_x^2}{2B_z^2} + \cdots\right)$$

Since B_x/B_z is of order 10^{-5}, we can ignore the second term of the expansion and consider only B_z. The field was mapped in the completed magnet via NMR along a helix about the z-axis near the midplane.

The results of such a map are shown in Figure 1 and can be fit using Legendre polynomials.[3] The dominant terms are presented in Cartesian coordinates where $R^2 = x^2 + y^2$:

$$B_z = B_0 + B_1 z + B_2 x + B_3 y + B_4\left(z^2 - \frac{1}{2}R^2\right) + B_5 zx + B_6 zy +$$
$$B_7\left(z^3 - \frac{3}{2}zR^2\right) + B_8\left(z^4 - 3z^2R^2\frac{3}{8}R^4\right)$$

The coefficients of the fit are presented in Table I. We see that the dominant terms are the x and y terms, which account for 3.4 ppm/mm. Furthermore, we can search a 1 cm DSV centered at the nominal field center using the fit coefficients and determine that the uniformity is 48 ppm.

The standard shimming procedure is to install wire-wound correction coils in the bore of the magnet. An alternative approach is to place small pieces of ferromagnetic material in the bore of the magnet. While shimming with correction coils might be possible, a two-step approach using ferroshims to get from 50 to 10 ppm, and correction coils to get from 10 to 1 ppm, requires less space. A bore tube was shipped to Resonance Research, who designed and built the ferroshim system consisting of numerous pieces of ferromagnetic material imbedded in the glass-epoxy on the outer surface of the bore tube. The ferroshimmed bore tube was returned and installed.

TABLE I
COEFFICIENTS OF FIELD INHOMOGENEITIES[a]

Term	No shims	Shims 0°	Shims 28°
z	-0.331	0.0915	0.0856
x	2.92	-0.414	-0.210
y	1.76	1.71	0.0868
z2	-0.0170	0.320	0.233
zx	0.181	-0.0301	0.0756
zy	0.0607	0.0629	0.0606
z3	-0.00219	0.0162	0.01714
z4	-0.00136	-0.00117	-0.00094
TLT[b]	3.41	1.76	0.227

[a] *Units are ppm/mm^n*
[b] *TLT denotes the Total Linear Transverse term, i.e. root of sum of squares of B_2 and B_3.*

While the ferroshims were being built, repairs were required on the magnet coils. Consequently, the bore tube as designed did not reduce the inhomogeneity as well as expected (Figure 1). By fitting the field maps with and without the ferroshims we were able to isolate the contributions from the coils and from the ferroshims and reoptimize the position of the ferrroshims. By rotating the bore tube 28 degrees counterclockwise we obtained a new, improved field profile as shown in Figure 1 and Table I.

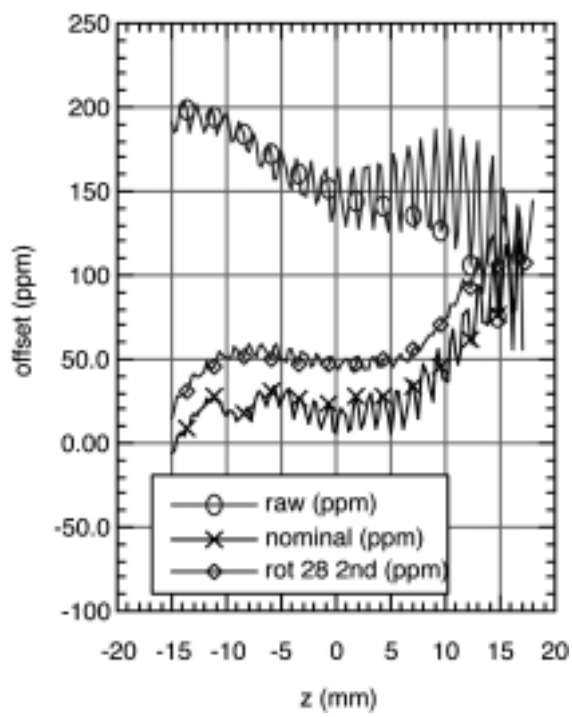

Figure 1. B_z from helical NMR maps for three cases: (1) magnet without ferroshims (raw), (2) magnet with ferroshims installed as designed (nominal), (3) magnet with ferroshims rotated 28 degrees counterclockwise (rot 28 2nd).

The ferroshimmed system presently has inhomogeneity of 12 ppm over 1 cm DSV as determined from the fit coefficients, an improvement of a factor of 4. The dominant term of the inhomogeneity in the unshimmed system was the pair of linear transverse terms, x and y. The net effect of these two terms has improved by a factor of 15.

Design of correction coils to reduce the inhomogeneity to 1 ppm is underway.

[1] Bird, M.D., *et al*., "Progress towards 1 ppm at 25 T," accepted by IEEE Trans. On Supercond.
[2] Bird, M.D., *et al*., IEEE Trans on Magn., **32**, no. 4, 2444-2449 (July 1996).
[3] Sauzade, M.D. and Kan, K.S., Advances in Electronics and Electron Physics, **34**, 1 (1973).

Axisymmetric Ferroshimming of High Field Magnets

Bird, M.D., NHMFL

An axisymmetric ferroshim for a high field magnet can be designed by considering a stack of rings of ferromagnetic material of uniform inner diameter located in the bore of the electromagnet. The outer diameter of each ring is a free parameter. The applied magnetic field (>2 T) takes each ring to its saturation magnetization and the field contribution from each ring can be easily computed at any point in space. A non-linear optimization algorithm can then be used to compute the outer diameter of each ring of material to shape the field as desired over some volume of space.

One application of this technology is to increase the uniformity of the field provided by the electromagnet. Such a shim was designed and built to be installed in a 50 mm bore magnet operating at 21.7 T at the NHMFL. Figure 1 shows a section of the shim including the steel and glass-epoxy filler used to keep the shim centered. Figure 2 shows a Hall probe map of the field along the axis both with and without the insert. We see that the inhomogeneity over a 6 mm diameter spherical volume has been reduce by a factor of 4. Such a system is inexpensive and easily installed compared with traditional approaches.

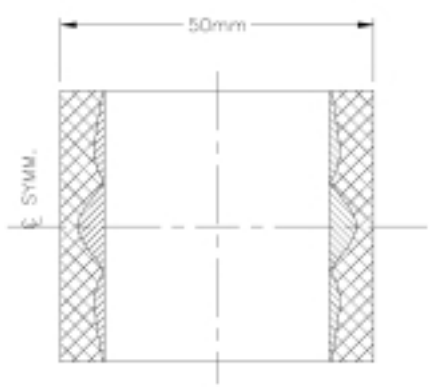

Figure 1. Profile of ferromagnetic insert for uniform magnetic field. Steel is shown with diagonal hatching, glass-epoxy is shown with cross-hatching.

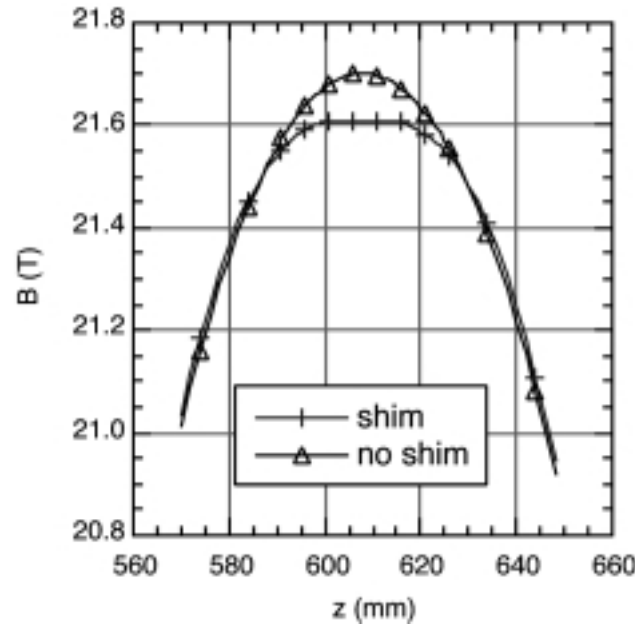

Figure 2. Measured on-axis field of 27 T magnet with and without high field uniformity insert.

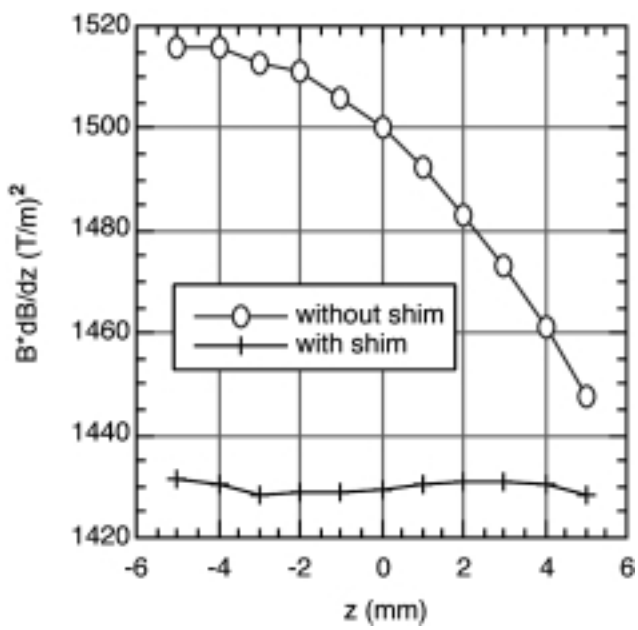

Figure 3. B_z*dB_z/dz computed along the axis of the 27 T, 50 mm bore magnet with and without uniform levitation insert.

Another application for axisymmetric ferroshims is in providing a space with uniform levitation force. Levitation of most biological materials requires a product of field and field-gradient to be around1400 T^2/m.[1] While most of the high field resistive magnets at the NHMFL provide greater than this amount, the levitation force can vary by as much as 10% over 5 mm. A second ferroshim has been designed for uniform levitation force and the computed levitation force with and without this insert is presented in Figure 3.

[1] Brooks, J.S., *et al*., "New opportunities in science, materials, and biological systems in the low-gravity (magnetic levitation) environment," submitted to 44th Conf. on Magn. and Magn. Mat., 1999.

Design of an Insert for Levitating Large Samples

Bird, M.D., NHMFL
Eyssa, Y.M., NHMFL

The magnetic body force vector, F, acting on a diamagnetic body in an applied magnetic field, B, is given:

$$\boldsymbol{F} = \chi\mu_0 (\boldsymbol{B} \cdot \nabla)\, \boldsymbol{B}$$

where μ_0 is the permeability constant. Biological materials have susceptibility, χ, around 9 X 10 $^{-6}$. To get a magnetic body force equal to gravitation requires the z-component of (B •∇) B to be around 1400 T^2/m. Most of the high field resistive magnets at the NHMFL produce a field-gradient product sufficient to levitate biological materials and near zero gravity experiments can be performed inexpensively on earth. Several experiments of this sort have been performed at the NHMFL and elsewhere.[1] Many of the proposed experiments, however, require larger levitation volumes than those presently available in our 32 mm and 50 mm bore magnets.

At the NHMFL we also have a 19.5 T, 195 mm bore magnet. Its field-gradient product, however, is not sufficient to levitate biological materials. We have examined ways of enhancing the field-gradient product of this magnet considering such possibilities as iron inserts, high-field insert coils, high-gradient insert coils, etc. It appears the optimal solution is to install a simple solenoid in the bore of the magnet above the midplane of the main coils as shown in Figure 1. Such a coil would certainly be resistive and would probably utilize Florida-Bitter technology.

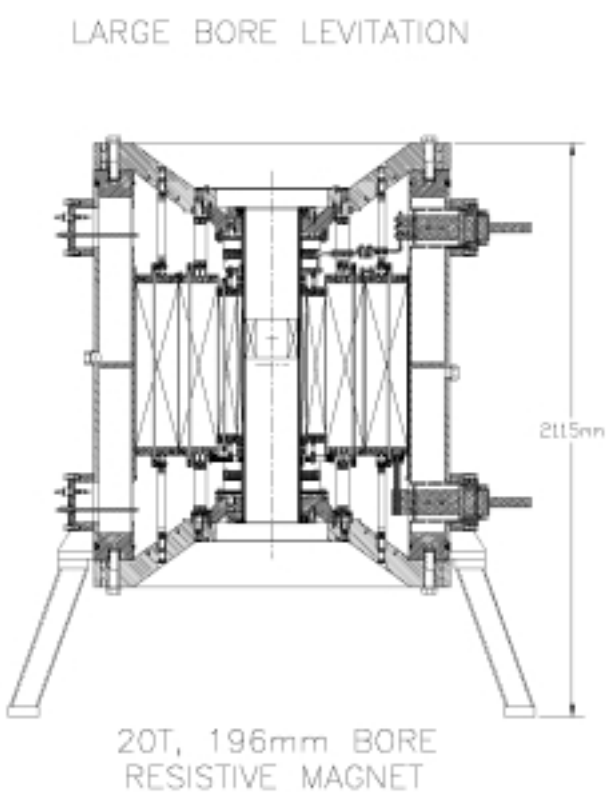

Figure 1. Configuration of large bore levitation system.

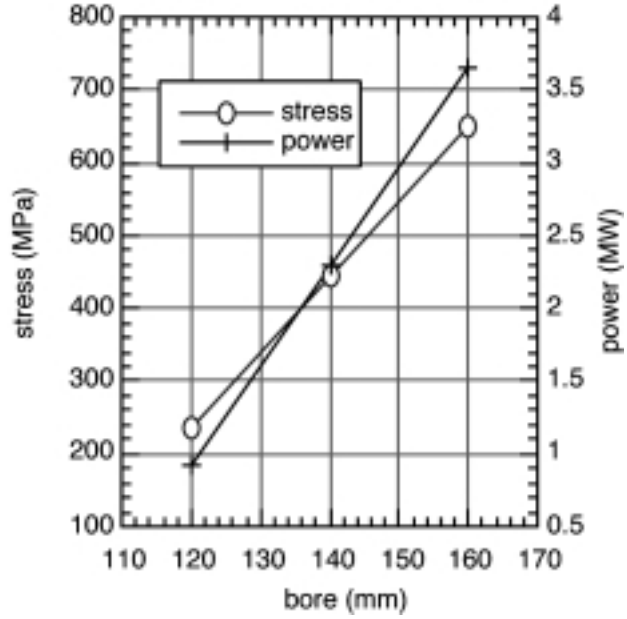

Figure 2. Computed power and stress versus bore of levitation coil installed inside of 19.5 T, large bore magnet.

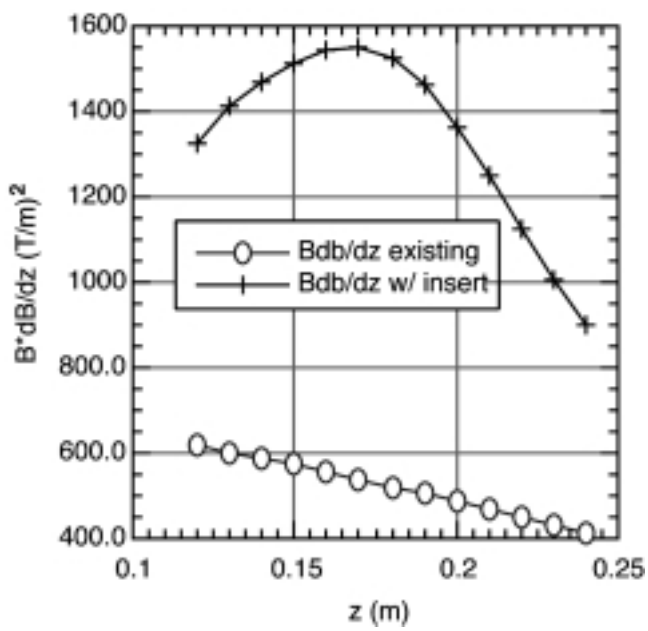

Figure 3. B_z*dB_z/dz computed along the axis of the 19.5 T large bore magnet with and without levitation insert coil.

By varying the inner diameter of the insert coil one can accomplish levitation over different volumes with different power requirements and stress levels. As the bore decreases, so do the power required and the stress in the conductor as seen in Figure 2. To keep the stress and power levels reasonable, the bore of the levitation insert will probably be 120 mm or less. It

should be noted that the main coils also generate a downward force on the insert coil of approximately 500 kN. The on-axis levitation parameter B_Z*dB_Z/dz is plotted in Figure 3 both with and without the insert.

[1] Brooks, J., *et al.*, "New opportunities in science, materials, and biological systems in the low-gravity (magnetic levitation) environment," Conf. Proc. 44th Mag. & Magn. Mat. Conf., 1999.

Variation of Critical Current with Transverse Pressure of a Rutherford Cable of Bi-2212

Dietderich, D.R., Lawrence Berkeley National Laboratory
Scanlan, R.M., Lawrence Berkeley National Laboratory
Aoki, Y., Showa Electric
Hasekawa, T., Showa Electric

There is much interest in using Bi-2212 in magnets for high energy physics applications due to the material's high upper critical field at 4.2 K. It is not known, however, if the material can withstand the high stresses (as high as 150 MPa) produced in dipole and quadrupole magnets during operation. Early measurements of critical current variation of Bi-2212 wire with stress showed that small loads (20-40 MPa) applied transversely to the wire would reduce the critical current of the wire by up to 80%.[1] If a Rutherford cable of Bi-2212 showed such a reduction there would be little hope of using Bi-2212 wire in accelerator magnet applications without some stress management.

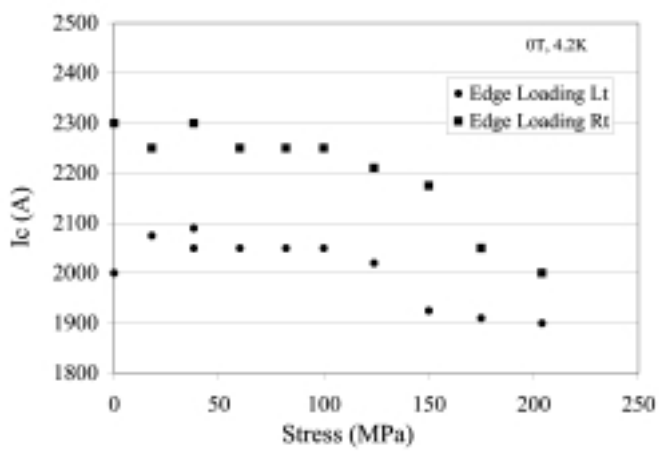

Figure 1. The critical current (0 T, 4.2 K) vs. stress for two cables loaded on the edge.

The first measurements of the variation of the critical current with load applied to a Rutherford cable of Bi-2212 are shown in Figure 1. No significant reduction is observed for stresses less than 100 MPa. The cable used in these measurements was heat treated on a form with a diameter of 200 mm. For testing the Bi-2212 cable was insulated with S-2 glass, placed into a 304 stainless steel fixture, and vacuum-epoxy impregnated to produce a robust assembly. This cable stack assembly simulates both the coil package and a react-and-wind process that one would use to produce a magnet.

[1] Ekin, J., Presented at the Low Temperature Superconducting Workshop, Sonoma, CA, Nov. 1-3, 1999.

Compressive Shear Strengths of NbTi Winding Composites with Various Insulation Sizing Agents, at 4.2 K

Dixon, I.R., NHMFL
Markiewicz, W.D., NHMFL
Walsh, R.P., NHMFL

The use of S-glass braid as wire insulation is fairly common for superconductors that require high temperature reactions, such as Nb_3Sn. It is not a standard product as insulation for more commonplace NbTi conductors. Its use, however, does have an advantage over traditional polyvinylformal insulation for large epoxy impregnated NbTi coils. The use of glass braid provides a means for a conductor to standoff from its neighboring turns and layers allowing epoxy to flow into regions that would otherwise be "gasketed" off. The glass braid also allows epoxy to soak deep into the windings.

Glass cloth products are usually manufactured with either an epoxy compatible sizing or a starch and oil sizing to help retain the fabric's integrity. Starch and oil is used in braid for Nb_3Sn conductors but is either cleaned off prior to winding the coil or burnt off during the heat treatment phase. Thus the starch and oil does not remain within the fibers by the time the epoxy impregnation process occurs.

An epoxy compatible sizing is an apparent choice for NbTi conductor insulation but its relative strength in comparison to insulation with starch and oil is generally unknown. NbTi winding composites have been manufactured for the purpose of measuring the shear strength as a function of insulation sizing.

Test Samples. The winding composites consist of straight lengths of NbTi wire in an array of 7 turns by 6 layers with a layer of E-glass cloth between conductor layers. The conductor has a rectangular cross section with dimensions of 0.938 mm x 1.595 mm. Three configurations of composites were made, one with epoxy compatible sizing, one with starch and oil sizing, and one with starch and oil sizing that was cleaned prior to the epoxy impregnation process. All composites were impregnated with NHMFL 61 epoxy.

A bi-axial, compression/shear strength test was employed. The fixtures are three components attached in series with the load path. The components have mating surfaces that are machined at an angle. The mating surfaces also have at their centers a recess where specimens are inserted. The test loads two samples simultaneously. A compressive force applied to the

fixtures is transmitted through the specimens contained within the recess, and is resolved into a shear force along the plane and a compressive force normal to the mating surface.

Results. Fixture angles of 45° and 15° were used. A summary of the test results is contained in Table 1. There is no evidence from the results, that any one sizing is better than the others. All samples failed at relatively high, but comparable, values. The use of starch and oil is not shown to reduce the epoxy bond strength to the fiber braid.

Table 1. Compressive shear test results of NbTi composites at 4.2 K, strengths in MPa.

Braid Condition	Fixture Angle	Shear Strength	Comp. Strength
EC	45°	92.7	92.7
EC	45°	127.0	127.0
EC	15°	62.9	16.9
EC	15°	60.6	16.2
Starch / Oil	45°	132.8	132.8
Starch / Oil	45°	132.0	132.0
Starch / Oil	15°	57.3	15.4
Starch / Oil	15°	55.2	14.8
Cleaned	45°	123.9	123.9
Cleaned	45°	133.4	133.4
Cleaned	15°	38.7	10.4
Cleaned	15°	57.8	15.5

Investigation of Plasticity Effects in a Pulsed Coil Using Finite Elements

Dixon, I.R., NHMFL

Verification of stress within the windings of an example coil is performed to confirm the existence of tensile axial stress. Linear analyses often show that under distributed axial compressive loads, the resulting axial stress is compressive. Highly loaded coils such as pulse magnets have shown that with plasticity effects included, a region of tensile axial stress exists. A study to verify the occurrence of axial stress using finite elements is performed.

The example coil that is considered is a 60 T pulse magnet. The coil consists of ten layers of Glidcop conductor with glass-epoxy inter-layer insulation and an exterior reinforcement shell constructed of A286. All layer heights are 98 mm, the inner radius is 12 mm, and the average current density is 2550 A/mm^2.

A magnetic analysis was initially performed to determine the distributed loading. The radial field through the first layer is positive throughout the entire area. Thus the axial force is directed toward the mid-plane, without any regions of positive loads. Results of the first two layers are presented. A contour plot of the axial stress is shown in Figure1. This does confirm the existence of tensile stress, toward the inner diameter of the coil. A plot of the stress along the mid-plane is given in

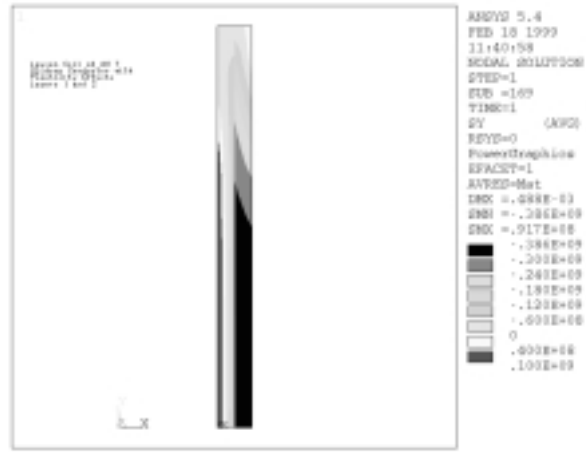

Figure 1. Axial stress contour plot of Layers 1 and 2.

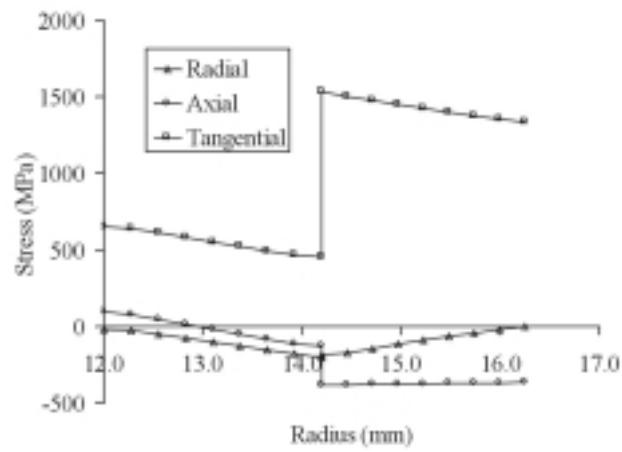

Figure 2. Stress distribution along the mid-plane of Layers 1 and 2.

Figure 2. The discontinuous curves show the location of the material discontinuity.

The tensile region in the axial stress occurs because the effective stiffness of the conductor is greatly reduced due to the plasticity effects and because of the Poisson's ratio effects. A linear analysis would reveal compressive stress everywhere because the modulus remains the same as the initial modulus. With plasticity a limit is reached on the stress yet the strain may still increase, which in turn reduces the effective modulus. From the stress strain relations

$$\sigma_z = \left[\varepsilon_z + \frac{\nu_{\theta z}\sigma_\theta}{E_\theta} + \frac{\nu_{Rz}\sigma_R}{E_R} E_z \right]$$

Thus the axial stress is directly proportional to the axial strain, which in this case is negative. The strain in the dominant loading direction, θ, however, is much more than it would be if it were a linear analysis, resulting in a greatly reduced effective (secant) modulus. This creates a relatively large positive stress component, which when all summed together, creates a positive, tensile axial stress.

Tests of Small Nb_3Sn Epoxy Impregnated, Wire Wound Superconducting Coils

Dixon, I.R., NHMFL
Markiewicz, W.D., NHMFL

Two superconducting test coils (SCTC's) have been manufactured to demonstrate some of the technologies developed for building superconducting coils at the NHMFL. The coils are relatively small, wound with Nb_3Sn conductor, and are epoxy impregnated. Table 1 contains some summary design and winding information of the coils.

Table 1. Test Magnet Parameters

Parameter	SCTC 1	SCTC 2
f_{Cu}	0.23	0.41
f_{SC}	0.69	0.53
wire height (mm)	1.10	1.10
wire width (mm)	1.80	1.73
IR (mm)	41.85	41.85
OR (mm)	72.00	72.00
L (mm)	45.00	45.00

The coils were tested with and without a background field to verify superconducting operation, heater performance, and design limits.

Design Limits. The design limit for the Nb_3Sn coils for the 900 MHz NMR magnet is 0.3% total strain, in the tangential direction. Demonstration of this strain level was exceeded with SCTC 2. The magnet was taken to 596 A, 114% of measured short sample J_C. A peak field in the windings of 12.9 T with a 7 T background field was produced. This results in a maximum strain in the windings of 0.41%.

Heater Performance. The main purpose of the quench tests is to determine the time required for the quench heaters to activate. As shown in Figure 1, a heater pulse is applied at time t_H for a period of approximately 1 second (t_H). The voltage drop that is produced across the heater strips increase with time

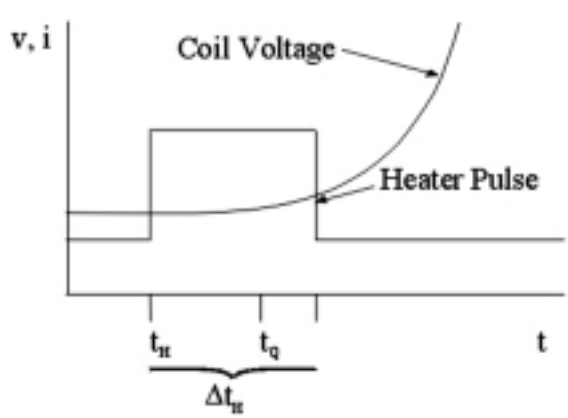

Figure 1. Schematic of heater pulse and voltage.

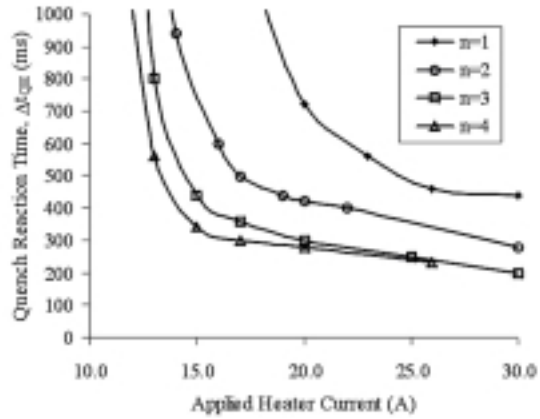

Figure 2. Quench reaction time for SCTC 2 as a function of applied heater current.

until the heater is fully activated, t_Q. The difference between t_Q and t_H, t_{QH}, is studied.

Tests were conducted to simulate a low current quench of the largest Nb_3Sn coil of the 900 MHz NMR magnet. At 50% of the operational current of 290 A, the heaters of the Nb_3Sn coil would be exposed to a magnetic field of approximately 5 T. The test coil was ramped to 145 A and with a background field the SCTC's heaters were at 5 T. Variations in the current applied to the heaters gave a picture the quench response time t_{QH}. Figure 2 shows the quench reaction time as a function of applied heater current and with a variation of the number of heater strips n.

Developmental Testing of HTS Shell Elements for High-Current Cryogenic Current Leads

Hodges, R., Eurus Technologies, Inc.
Richardson, D., NHMFL
Miller, G., NHMFL
Miller, J.R., NHMFL

The NHMFL and Eurus Technologies, Inc. are engaged in a cooperative research and development agreement (CRADA) to develop high-current cryogenic current leads for large magnet systems. A specific long-term goal of this collaboration is to produce a pair of 20-kA leads for a next-generation hybrid magnet system for the NHMFL, and a near-term goal is to demonstrate the relevant technologies for such leads in a pair of 13-kA leads appropriate for the Large Hadron Collider at CERN in Geneva. The present approach to lead designs for both these applications is to combine a large number of high-temperature superconductor (HTS) tapes into a cylindrical shell element such as that pictured in Figure 1. A full current lead would incorporate several of these nested coaxially. The HTS tapes in this case are based on BiSCCO-2223 with a Ag-18at%Au matrix, and the cylindrical shell incorporates an integral stainless-steel shunt for protection in case of a

quench of the HTS. Critical issues are the degree of current sharing among tapes that can be achieved in such an element and the effective critical current in the presence of self-field. Current elements such as pictured in Figure 1 were tested in the NHMFL's Large Magnet Component Test Facility. Data for a typical test are displayed in Figure 2 with a fit to the simple relation $V = V_{offset} + I \cdot R_{dc} + V_0 \cdot (I/I_0)^n$. Fit parameters are as follows:

$V_{offset} = 3$ mV
$R_{dc} = 1\ \mu$
$V_0 = 20\ \mu$V,
$I_0 = 1010$ A, and
$n = 7.9$.

Figure 1. Photograph of a typical cylindrical HTS shell element for a high-current, cryogenic current lead, ready for testing.

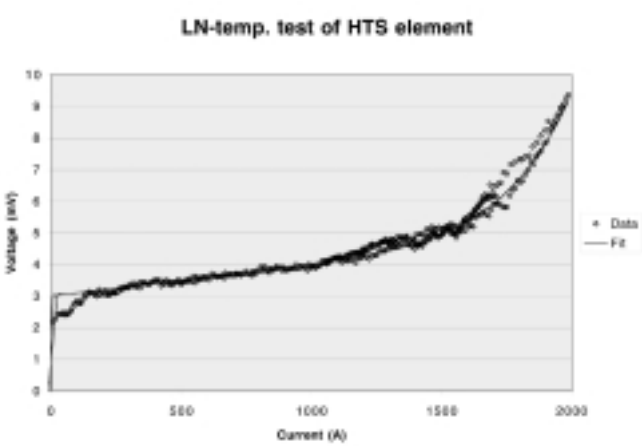

Figure 2. Plot of typical measurements of total voltage across a shell element vs. imposed current at 77 K and self field, including fit.

Preliminary Tests of High-Current, Cryogenic Current Leads for the CERN LHC Project

Hodges, R., Eurus Technologies, Inc.
Richardson, D., NHMFL
Miller, G., NHMFL
Miller, J.R., NHMFL

The NHMFL and Eurus Technologies, Inc. have collaborated on the development of high-current, cryogenic current leads for the Large Hadron Collider (LHC) at CERN in Geneva. Figure 1 shows a photograph of one of these leads, rated at 13 kA, prior to delivery. These leads have critical interfaces between the gas-cooled, resistive portion and the high-temperature-superconductor (HTS) element and also between

Figure 1. Photograph of a 13-kA, cryogenic current lead built for the LHC in CERN.

the HTS element and the low-temperature-superconductor (LTS) element. One aspect of the NHMFL's responsibility has been to perform preliminary tests of these critical interfaces at high current and cryogenic temperatures in its Large Magnet Component Test Laboratory. Figure 2 displays data of the simultaneous test of these interfaces on two separate leads (A and B) at LHe temperature in self-field. The monitored sections of each lead were labeled as follows: a-b is between the bottom of the gas-cooled resistive and a copper plate to which the HTS elements were attached, b-c is between the copper attachment plate and the middle of the HTS element, and c-d is between the HTS element and the LTS element. Fits to the data show that the highest resistance is approximately 20 n on one of the HTS/LTS interfaces, which is just within the allowable range.

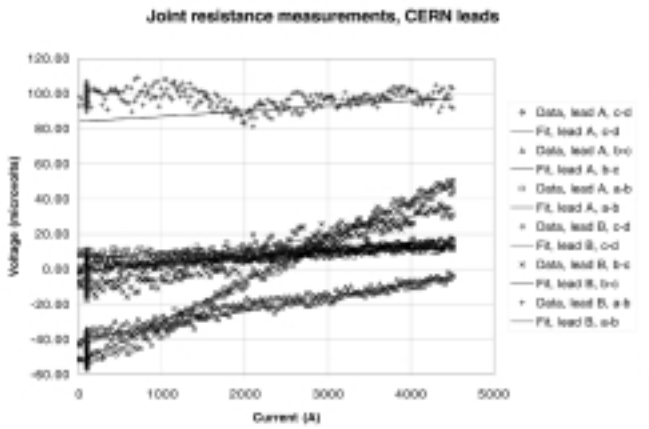

Figure 2. Plot of voltage measurements across critical interfaces in the LHC current-lead pair vs. imposed current at 4.2 K and self field. The labels indicate the following: a-b, gas-cooled resistive part to HTS-element connector plate, b-c, connector plate to middle of HTS element; and c-d, HTS element to LTS element.

All other interfaces are significantly smaller, in some cases by an order of magnitude or more.

Ramp-Rate Limitation Experiment Using a Dipole Magnet

Jeong, S., Korea Advanced Institute of Science and Technology
Miller, G., NHMFL
Whitton, M., NHMFL
Van Sciver, S.W., NHMFL/FAMU-FSU College of Engineering
Miller, J.R., NHMFL

This report describes a methodology of performing a ramp-rate limitation (RRL) experiment using a background magnet only without an additional power supply for the CICC (Cable-In-Conduit Conductor) sample. The TACL (Test of AC Loss) facility of the NHMFL was used as a background magnet and the hair-pin shape loop sample with a G-10 spacer was tested by using the induced current in a changing magnetic field. The electronic circuit diagram of this experiment is shown in Figure 1. The current was induced in the sample loop by magnetic coupling. Adjusting the flux linkage area of the sample with the dipole magnet and the magnitude of the shunt resistor controls the maximum induced current. The inductance and the resistance of the sample were carefully selected to create a large enough steady current for quenching the sample during the field ramp. A calibrated shunt resistor (about 2 μ) in the sample loop could measure the sample current precisely. In our first experiment, 1.95 kA was generated by magnetic coupling in the sample loop at 1 T/s ramp of the magnet. Figure 2 shows the experimental data for different ramp rates of the magnet. In spite of the precise alignment of the sample to the magnet, the experimental data of Figure 2 (b) showed that the induced current was not staying constant, which means that the sample was twisted due to the large torque generated by Lorentz

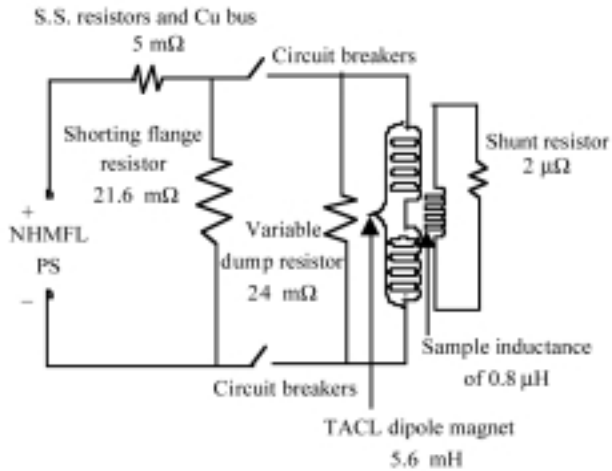

Figure 1. Electronic circuit diagram of the ramp-rate limitation experiment.

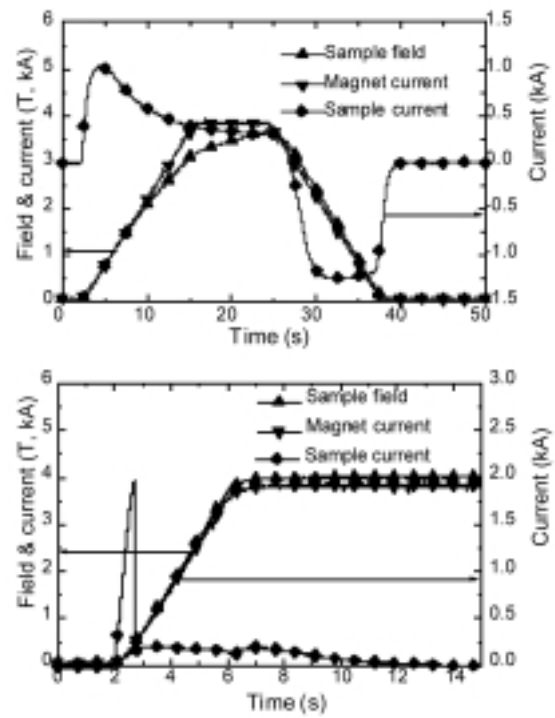

Figure 2. Experimental data with dB/dt of (a) 0.05 T/s, (b) 0.3 T/s, (c) 1.0 T/s.

force. The force balance analysis of the sample after the experiment could explain the generated current quantitatively. The hypothesis of torque generation was strongly supported by the negatively induced current during the field ramp-down as shown in the rear part of Figure 2 (b). When the field was going down, no torque was generated because the Lorentz force was exerted outward. Trying to pull apart the U-shape legs of the sample, the Lorentz force created no torque. With an improvement of the sample joint and the rigidity of the sample structure, the proposed methodology in this report should be appropriate for the future RRL experiment of large superconducting cables.

Test of HTS J Bars for the General Atomics Fault Current Limiter

Leung, E., General Atomics Corporation
Miller, G., NHMFL
Miller, J.R., NHMFL
Romans, J., Eurus Technologies, Inc.

General Atomics Corporation (GA) was leader of a team responsible for delivering a superconducting fault-current limiter to Southern California-Edison (SCE) as part of the overall U.S. Department of Energy Program on Superconductivity in Electric Systems. GA's system is based on large inductors built with high temperature superconductors (HTS). Critical components include the superconducting busbars (called J bars because of their shape) that connect the inductors internally to the cryostat. These J bars also use HTS, in this case Ag-matrix, BSCCO-2223 tapes, and were supplied by Eurus Technologies, Inc. To confirm their performance prior to shipment and incorporation into the overall system, the team requested testing at the NHMFL's Large Magnet Component Test Facility. These tests were carried out and reported to the team. Three J bars were tested and all performed quite similarly. Typical test data are shown in the figure below, which records total J-bar voltage vs. current at 77 K and self field. The data are fit to a form $V = I \bullet R_{dc} + V_0 \bullet (I/I_0)^n$ with the following results:

$R_{dc} = 0.068\ \mu$
$V_0 = 10\ \mu V$,
$I_0 = 1550$ A, and
$n = 7.9$.

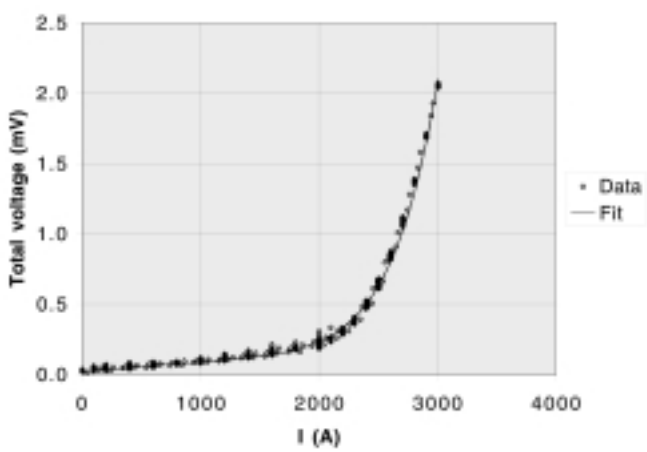

Figure 1. Plot of typical measurements of total J-bar voltage vs. imposed current at 77 K and self field, including fit.

Eddy Current Loss Analysis in the High Field Pulsed Magnet with Conductive Reinforcements IHRP

Li, L., NHMFL
Eyssa, Y., NHMFL
Lesch, B., NHMFL
Cochran, V.G., NHMFL
Stanton, R., NHMFL

In the recently developed pulsed magnets, conductive reinforcement shells are introduced in the construction to compensate the anisotropic mechanical properties of the fiber composite materials. During the discharging, eddy current will be induced in the conductive shells made of MP35N. For a system of magnetically and electrically coupled circuits, the equation for each circuit can be written as:

$$\frac{d^2 I_i}{dt^2} = \frac{1}{L_i}\left(\frac{I - I_c}{C_i} - R_i \frac{dI_i}{dt} - I_i \frac{dR_i}{dt} + \frac{dV_m}{dt} + \frac{dV_e}{dt}\right) \qquad (1)$$

where L_i, R_i and C_i are the inductance, resistance and the capacitance of circuit i respectively. The induced voltage V_m representing the coupling of the circuit with the others can be expressed as

$$V_m(i) = \sum_{j=1}^{n} M(i,j)\frac{dI(j)}{dt} \qquad (2)$$

with M(i,j) the mutual inductance between circuit i and circuit j, which can be calculated from their relative positions and the coil geometry. The V_e in the Equation (1) reflects the coupling of the circuit with all the magnetic flux generated by the eddy current loops. This can be calculated by a magnetic diffusion analysis. A computer code has been developed to solve the equations numerically.

Taking the coil ZY103 as an example, Figure 1 shows the computed and experimental peak field versus the capacitor bank energy. The result in which the eddy current in the shell

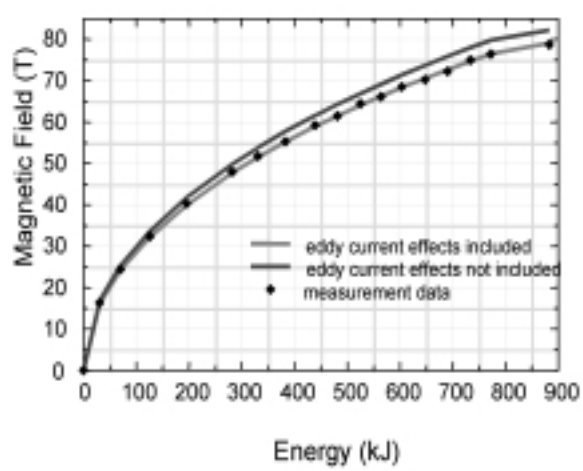

Figure 1. The calculated and experimental peak field versus the capacitor bank energy of the coil ZY103.

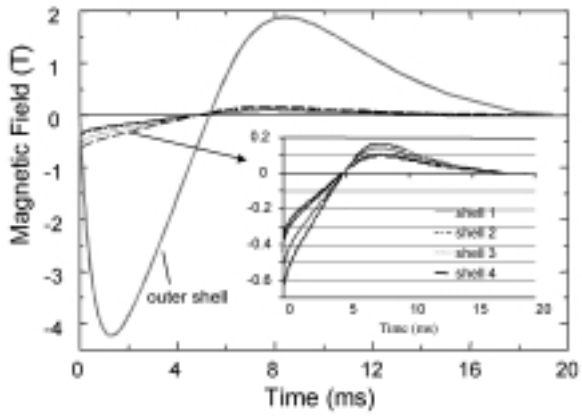

Figure 2. The calculated fields produced by the eddy current in each conductive shell of the coil Zy103 as a function of time in a 79 T pulse.

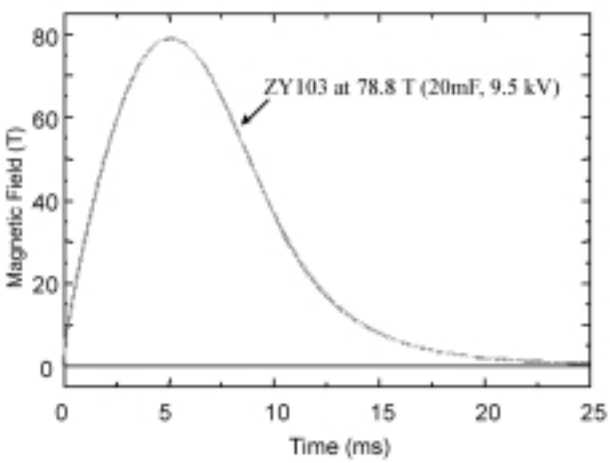

Figure 3. Waveform of a 79 T pulse measured in the coil test.

is considered shows a good agreement with the measurement during the coil testing. The magnetic field caused by the eddy current flowing in the shells is shown in Figure 2. It can be noticed that at the time when the total field as shown in Figure 3 reaches the peak (at about 5.1 ms), the magnetic field from the eddy current in the shell is close to zero. This indicates that the field reduction is caused by the energy consumed in the conductive shells instead of the negative field produced by the eddy currents.

Synchronous Digitization High Speed Lock-In System

Migliori, A., NHMFL/LANL
Betts, J.B., NHMFL/LANL
Balakirev, F.F., NHMFL/LANL
Boebinger, G.S., NHMFL/LANL

The unique electrical and thermal noise environment of high-magnetic-field experiments typically introduces additional noise into measurements that is not information theory limited.[1] Rather, the use of general-purpose laboratory instruments (voltmeters, amplifiers, lock-in detectors and spectrum analyzers) at the edge of their design envelope is a more common culprit. This is particularly true for pulsed magnetic field experiments, for which the marketplace does not develop instrumentation adequately tailored to the magnetic field pulses. Key to overcoming such design problems are the astonishingly low-noise, high-dynamic-range, high-bandwidth operational amplifiers only recently available, as well as chip-level high speed digitizers, board-mounted microprocessors, and modern digital signal processing algorithms.

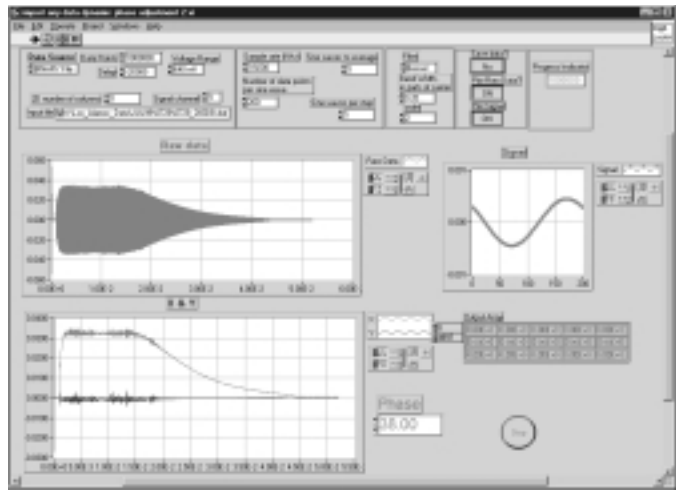

Figure 1. The LabView interface for the NHMFL S-D Lock-in. Shown are in-phase and quadrature signals from a resistance measurement in the 60 T short-pulse magnet illustrating post-shot adjustment of phase and time constant, with a S/N ratio 35 times better with faster response time than the commercial lock-in previously used.

We have designed and fabricated a coherent synthesized AC excitation source used to drive commercial high-speed digitizers at an integral multiple of the sine-wave excitation frequency (synchronous-digitization lock-in) used for a typical lock-in measurement. The synchronous digitization provides zero settling time of the lock-in. Digital signal processing with information-theory-limited acquisition speeds has been demonstrated. Results indicate as much as a 35-fold improvement in signal-to-noise in a short pulse magnet experiment, completely replacing the conventional lock-in amplifier. Furthermore, the extreme dynamic range and bandwidth have resolved features masked by the time-constant constraints of conventional lock-in techniques, and can improve on measurements made in DC magnets as well. A commercially manufactured unit (using NHMFL designs and under NHMFL direction) is now available at substantially lower cost than the conventional laboratory instruments it will replace. This technique and associated hardware can be run from a LabView interface and is expected to improve data acquired during a broad range of measurements now using lock-in techniques in pulsed and DC fields.

[1] Migliori, A., and Sarrao, J.L., *Resonant Ultrasound Spectroscopy*, John Wiley, New York, 1997.

Calorimetric Measurement of Energy Dissipation in Superconducting Cables

Minervini, J.V., Massachusetts Institute of Technology, Plasma Science and Fusion Center
Alvey, T.D., MIT, Plasma Science and Fusion Center
Takayasu, M., MIT, Plasma Science and Fusion Center

An experimental study of energy dissipation, also know as AC loss, was carried out on a 36-strand subsized Cable-In-Conduit Conductor (CICC) of Nb_3Sn superconducting wires used for the International Thermonuclear Experimental Reactor (ITER) Central Solenoid (CS) Model Coil, in order to understand AC loss mechanisms of a large-scale superconducting magnet. AC losses were measured using an isothermal calorimetric method. Testing was performed using the 20 T, 200 mm large bore magnet. The magnet produced a small amplitude, sinusoidal ripple field of up to 4 Hz superimposed on a DC bias field by modulating the magnet power supply. AC losses were evaluated as a function of ripple frequency at constant ripple amplitude with various DC background fields. Ripple field losses were also measured with transport currents ranging from 0 to 6 kA. The test regimes simulated transverse Lorentz force loading conditions of the ITER CS model coil magnet. Measured AC losses increased by a factor of approximately 3.75 when measured as a function of ripple frequency, from 1 to 4 Hz, at a constant background field and no applied transport current. This is consistent with the expected increase of a factor of 4. An increase of Lorentz loading from 0 to 48 kN/m resulted in a 40% increase in the measured AC loss. The cable coupling current time constant at zero current declined after cyclic Lorentz force loading, from 20 ms in the virgin state to 6 ms after several cycles.

Acknowledgement: This research was supported by the U.S. Department of Energy, Office of Fusion Energy Sciences under grant DE-FG02093ER54186.

Conceptual Design of a Muon-Electron Conversion Experiment

Prestemon, S., NHMFL/FAMU-FSU College of Engineering
Van Sciver, S.W., NHMFL/FAMU-FSU College of Engineering
Eyssa, Y., NHMFL
Crook, D., NHMFL
Liu, T. J., Univ. of California, Irvine, Physics
Molzon, W., Univ. of California, Irvine, Physics
Sculli, J., New York Univ., Physics

The NHMFL has concluded a design study for the Muon-Electron Conversion Experiment (MECO) magnet system. The proposed experiment will search for violation of additive quantum numbers, often referred to as "lepton flavor violation". Such a violation is anticipated by a number of extensions to the Standard Model, and its detection would have a significant impact on the direction of particle physics research. The experiment will use a high energy proton beam provided by the AGS located at Brookhaven National Laboratory.

The experiment consists of the search for the process $\mu^- N \rightarrow e^- N$ with very high sensitivity. If the process occurs, the resulting electron will have an energy of ~105 MeV. The experiment requires the abundant creation of μ particles, their transport to a stopping target and the precise detection of an electron of given energy emanating from a decay process.

The system, as shown in Figure 1, is essentially composed of three solenoidal field sections, the first being the production solenoid, where the μ particles are created by impacting a tungsten target with accelerated protons. This is followed by the transport solenoid, which includes two 90° bends serving to select particles of the correct sign and momentum. Finally, the detector solenoid is a 10 meter long section with a large bore containing the stopping target and the detector and instrumentation. The peak field of 3.3 T occurs in the target solenoid. From there the field must decrease in a prescribed, monotonic shape along the beampath, culminating in a 1 T field with 10^{-4} homogeneity in the detector region.

Due to the nature of the experiment, the field quality must take precedence over other design issues in order for the experiment to be successful. Each section of the three-section system is assumed to consist of consecutive solenoids of equal inner radii. In order to reduce/eliminate field gradient reversals, the space between consecutive coils is minimized. In the straight sections the coils are therefore touching, while in the bent sections a minimal spacing is applied to the coils on the inner bend radius to allow control of the coil placement as well as the forces acting on them.

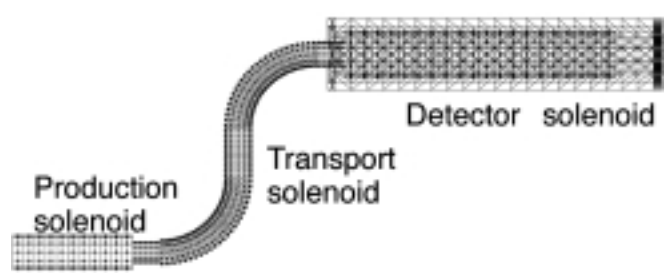

Figure 1. View of the MECO magnet system. The detector solenoid is encased in a large iron shield to reduce the possibility of cosmic-ray interference.

Although the forces on the magnets (both from the Lorentz forces and weight) are not particularly large, numerous other elements must be supported inside the solenoid bores. The production solenoid must contain a 29 metric ton radiation shield. The transport solenoid contains collimators in each of the straight sections, and the detector solenoid contains a

stopping target as well as the detector itself. Finally, throughout the whole system an uninterrupted warm vacuum tube must be supported. The only coil separations that occur are in the bent sections; the resulting field oscillations are minimized by the discretization into many small coils, and field reversals are eliminated by imposing a field gradient.

Magnet System Design With Cost Optimization

Prestemon, S., NHMFL/FAMU-FSU College of Engineering
Miller, J., NHMFL
Eyssa, Y., NHMFL
Green, M., Lawrence Berkeley National Laboratory

The NHMFL has performed a number of design studies for Fermi National Laboratory concerning magnet systems for the Muon-collider group. Due to the scale of the systems involved, it is crucial that system cost be minimized, while satisfying the field requirements stipulated by the physics.

We consider here the problem of optimizing the design of magnet systems to simultaneously satisfy a set of constraint equations for field, geometry, protection, and stability while minimizing the total system cost. We describe an algorithmic approach that allows us to incorporate cost directly into the conceptual design of a magnet system. There are numerous advantages to such an approach. First, the designer has direct access to an estimate of the system cost, which, although only approximate, is useful as a reference point. Second, by modifying each of the system variables and re-evaluating the desired field values and the system cost, the designer can gain a feel for the effect of each variable and isolate those that are critical from a cost and/or field perspective. Such information is often not available in traditional design practice.

The basic premise of our approach is that magnet design optimization and magnet cost can and should be integrated into a single process. We assume that the underlying design optimization problem can be written in the form

$$\underset{x \varepsilon \Omega}{Min}\ [F(\vec{x})]\ with \begin{cases} G_i(\vec{x}) = 0,\ i = 1, n \\ H_j(\vec{x}) \geq 0,\ j = 1, m \end{cases}$$

The function F will be called the field function, and will typically describe the deviation of the field from the desired profile. For solenoids the variable $\vec{x}$ typically contains such quantities as magnet geometry (inner and outer radius, height) and average current density. Constraints of the form G and H are commonly encountered in design problems, and may represent such quantities as stress, strain, power, or geometric restrictions.

A solenoid represented by the variable $\vec{x}$ will be assumed to have an associated cost defined by $C=C(\vec{x})$. The cost will depend on such quantities as material volumes, magnet technology being applied, and fabrication processes characterized by conductor length, coil volumes or mass, etc; the calculation of $C(\vec{x})$ is in reality often the solution to a minimization problem itself.

We propose a new objective function Γ defined by $\Gamma=F+\lambda C$, where λ is weight factor that defines the relative importance of cost to field profile for a given application. Minimizing Γ results in a magnet that approaches the ideal field profile while taking into account system cost. Moreover, the gradient $\nabla\Gamma$ yields insight into the relative importance of each variable to the overall minimization process, and since F and C are distinct functions, the designer can evaluate the relative ratios

$$\rho_i = \frac{\delta F / \delta x_i}{\delta C / \delta x_i}$$

that distinguish a variable's effect on field profile and cost. The values ρ_i should play an important role in magnet system design: a small ρ_i value implies that significant cost savings can be obtained without significant influence on the field profile.

This work has led to the development of software that couples in-house costing algorithms and design optimization codes. The resulting code will significantly aid in the design of magnet systems for the Muon-collider project, as well as many other projects involving large magnet systems.

Data Analysis for the CICC Model Coil of the Indian Institute for Plasma Research

Sayre, S., FAMU-FSU Computer Science and Software Engineering
Prestemon, S., NHMFL/FAMU-FSU College of Engineering
Luongo, C., NHMFL/FAMU-FSU College of Engineering
Miller, J., NHMFL

This is a collaborative research effort between NHMFL and the Indian Institute for Plasma Research (IPR). The present activities are expected to conclude in early 2000. The scope of the effort is to utilize the NHMFL's magnet design tools and expertise to analyze experimental data obtained by IPR on a model coil relevant to the design of SST-1, India's experimental fusion device. The model coil was wound with essentially the same full-scale conductor to be used in SST-1, a nominal 10 kA cable-in-conduit conductor (CICC) made of NbTi strands for operation at 5 T and 4.5 K (supercritical helium). The model coil consisted of 8 double pancakes with the following approximate dimensions: 36 cm inner diameter, 72 cm outer diameter, and 28 cm height. To simulate the actual conditions that will be experienced by the conductor in the fusion device, the model coil was placed inside a 4-coil toroid producing

a longitudinal pulsed field, while a pair of central bucking solenoids placed on the model coil's inner bore were used to generate a pulsed transverse field. Stability and quench data were gathered on a series of tests under different conditions of current and pulsed fields.

The NHMFL was given information on the test setup and procedures, as well as a voluminous amount of data corresponding to the entire experimental campaign. NHMFL's scope of work consisted of: (a) creation of a hydraulic model, (b) creation of a magnetic model, (c) data reduction and interpretation, (d) computer simulation of quench and comparison with experiment, (e) conclusions and recommendations. The first step was to create a hydraulic model of the CICC test coil to be used in the quench simulations. The model was derived from information on the coil geometry, including joint locations, hydraulic path terminations and manifolds, and CICC dimensions. The model also included the details of instrumentation locations, including voltage taps, for subsequent correlation with the test data. It was determined that the only test runs of interest were those in which the model coil had been quenched as a result of the external pulsed magnetic field generated by the 4-coil toroid and the central solenoids. Detailed magnetic field computations were carried out to determine the three-dimensional field distribution on the model coil due to its own current, as well as from the external pulsed coils. The magnetic field distribution was then converted to an AC loss distribution used to simulate the stability tests and infer quench initiation conditions. In parallel with these activities, the experimental data were processed, plotted, and analyzed. It was determined that only a few of the runs in the experimental campaign contained enough useful stability and quench information. The computer simulations were concentrated on these test runs. Figure 1 shows the magnitude of the peak toroidal field contribution parallel to the conductor for the centermost double pancake. Close inspection reveals four peaks, corresponding to the four toroidal magnets, for each of the 12 turns in each pancake. The inset magnifies the region around the center of the path, corresponding to the switchover from the innermost turn of the bottom pancake to the innermost turn of the upper pancake. A similar distribution can be inferred for the perpendicular component of the field. The intricate field distribution leads to a rather complex quench initiation and propagation scenario that will be elucidated through computer simulation to help interpret the experimental data.

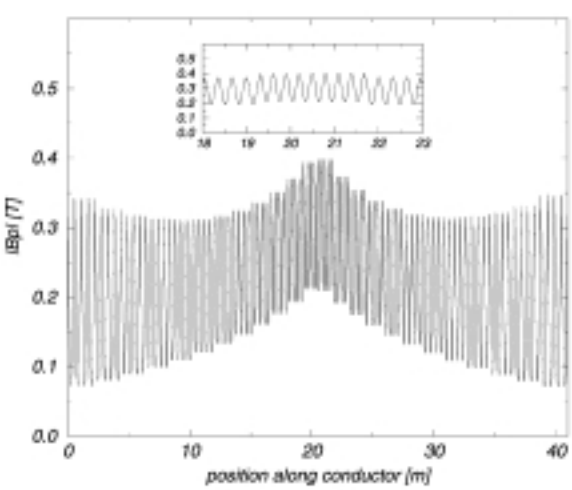

Figure 1. Field component parallel to the conductor along the length of a hydraulic path.

The final two phases of this effort are ongoing. Simulations of the model coil quenches are being done with the computer code Gandalf applied to the hydraulic model subject to the calculated magnetic field profiles. These simulations will be compared with the experimental data in order to confirm some of the quench initiation and propagation scenarios as gleaned from the data (there were not enough voltage taps to fully follow the normal front propagation). Matching the data with computer simulations will also allow us to roughly infer the AC loss time constant for the SST-1 conductor. Based on the present work, we will suggest improvements to future experimental setups and instrumentation schemes to be implemented as part of India's fusion research program.

$Bi_2Sr_2Ca_2Cu_3O_x$ Conductor for High Field Insert Coils

Weijers, H.W., NHMFL
Schwartz, J, NHMFL/FAMU-FSU College of Engineering

As part of the ongoing effort of the NHMFL to develop the technology for high field insert coils using high temperature superconductors, intended for 25 T NMR, we have constructed two $Bi_2Sr_2Ca_2Cu_3O_x$ (Bi2223) react-and-wind double pancake coils and tested them in background fields of up to 19 T.

Reacted conductor from two sources was used: Bi2223 conductor with a mixed silver/silver-alloy (AgMg) matrix from Nordic Superconductor Technologies A/S (NST) and conductor with a pure silver (Ag) matrix from the Korean Institute of Machinery and Materials (KIMM). The Ag-sheathed conductor has a yield point of about 50 MPa at cryogenic temperatures versus about 150 MPa for the alloyed conductor. Double pancake coils with inner/outer diameters of 97/127 mm were wound on a thin ceramic bore tube, using Kapton tape as turn-to-turn insulation. Vacuum-impregnation with epoxy consolidated the coils. Each coil was thermally cycled and tested twice at 4.2 K, in self-field conditions before in-field testing in the 19 T large bore resistive magnet at the NHMFL.

In both coils a small degradation of 1-2% of I_c was observed with every thermal cycle. Short samples do not have this behavior. The critical current of both coils was reversibly reduced to about 1/3 of the short sample value by a background field of 19 T. After reaching I_c at 19 T, the operating current was further increased, and thereby the Lorentz-force induced stress and strain on the conductor, until irreversible degradation occurred. Irreversible degradation is associated with exceeding

the yield point of the conductor, about 0.18% and 0.35% respectively for the used Ag and AgMg sheathed conductor. The degradation, in both coils, first occurred in the inner turns, even though the local Lorentz-force is higher on the outer turns. This indicates that there is sufficient mechanical coupling between the turns to transmit radial loads. The AgMg conductor reached its yield point when the sum of the bending strain and Lorentz-force induced strain reached 0.35%. The Ag conductor, bent to a radius that already caused some of the filaments to exceed their yield point, could handle an additional load of almost 50 MPa before the inner turns showed irreversible degradation. It appears as if the effect of bending and Lorentz-force induced strain is cumulative for the AgMg conductor, whereas in Ag sheathed conductor they can be considered separately. This difference is understood in terms of the mechanical properties of the conductors. The Ag matrix is soft and yields upon bending, releasing the stress between filaments and the matrix. The AgMg matrix behaves elastically, retaining the stress between filaments and matrix after bending. Despite this retention, the AgMg conductor handles larger Lorentz-force induced loads.

In addition, short samples of a different batch of NST conductor were tested in a 30 T resistive magnet at the NHMFL and found to carry an engineering current density of 180 A/mm^2 at 30 T, with an n-value of 15. Considering the typical requirement of 70-100 A/mm^2 for high field NMR inserts, there is still a fair margin for insulation and external reinforcement. In sufficient lengths, this is useful conductor for high-field insert magnets.

Development and Testing of a 3 T $Bi_2Sr_2CaCu_2O_x$ Insert Magnet in a 19 T Background

Weijers, H.W., NHMFL
Celik, E., NHMFL
Hascicek, Y., NHMFL
Hu, Q., NHMFL
Viouchkov, Y., NHMFL
Schwartz, J., NHMFL/FAMU-FSU College of Engineering

As part of the ongoing effort of the NHMFL to develop the technology for high field insert coils using high temperature superconductors intended for 25 T NMR, we have constructed a 3 T $Bi_2Sr_2CaCu_2O_x$ (Bi-2212) insert magnet and tested it in background fields up to 19 T.

The design of the magnet is based on three stacks of double pancakes of Bi-2212 powder-in-tube tape conductor produced by Oxford Superconducting Technology Inc. and using the wind-and-react approach. This choice was motivated by the success of a 1.2 T single-stack insert coil reported in the 1997 NHMFL Annual Report. For the 3 T coil, three concentric sections were used, labeled A, B, C from the inside out. The number of double pancakes was increased to achieve the desired additional central field of 3 T. The inner section used conductor with a pure Ag matrix, the outer sections a matrix with a mix of pure Ag and AgMg alloy. Each section was powered using a separate power supply. As a whole, the coil was 131 mm in diameter and 98 mm tall. All testing was performed at 4.2 K in the large bore resistive magnet at the NHMFL.

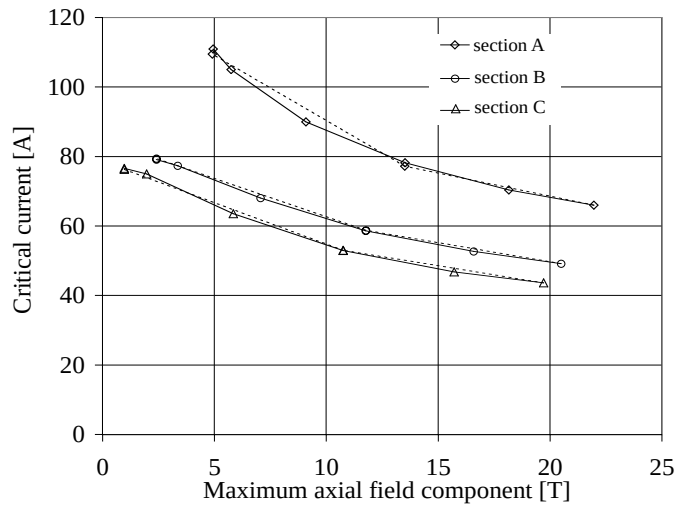

Figure 1. Measured critical currents in the 3 T insert magnet as a function of the maximum axial field component in each section. The lines connecting the datapoints are a guide to the eye only. Dashed lines connect datapoints taken while reducing the background field.

The HTS magnet generated 4.6 T at self field and 3.0 T, the design goal, in a background of 19 T. The average current densities in the windings were 86, 57, and 51 A/mm^2 respectively for the A,B,C sections at 19+3 T. This approaches design values of 70-100 A/mm^2 typical for high field NMR applications. The behavior of the critical current as a function of field, shown in Figure 1, can be modeled using short sample data and the critical currents of the double pancakes before stacking. The critical currents were found to be determined by the axial field components, except in background fields below 2 T for the B and C stacks. The calculated strain in each section of the magnet was well below the critical value, indicating that the conductor is mechanically capable of operating at higher current densities and radii without additional reinforcement.